

<https://doi.org/10.1038/s43247-024-01332-8>

Exacerbated summer European warming not captured by climate models neglecting long-term aerosol changes

Check for updates

Dominik L. Schumacher , Jitendra Singh , Mathias Hauser , Erich M. Fischer , Martin Wild & Sonia I. Seneviratne

In much of western-central Europe, summer temperatures have surged three times faster than the global mean warming since 1980, yet this is not captured by most climate model simulations. Here we disentangle this warming into thermodynamic and circulation-induced contributions, and show that the latter is the main reason why numerically simulated warming is weaker than observed. Crucially, regional climate models from the Coordinated Regional Downscaling Experiment with constant aerosol forcings systematically show the strongest discrepancies from observations: in these simulations, the regional brightening and associated thermodynamic warming due to aerosol reductions is not represented. We estimate an effect of ~ 0.5 °C over western-central Europe for our model ensemble, and the discrepancy to climate models with evolving aerosols increases in future projections. To better reap the benefits of regional high-resolution simulations, it is thus imperative to represent the relevant external forcings and associated responses across the entire climate model chain.

There is a growing demand from society for reliable long-term climate projections, from global to regional and local scales. Ongoing and future climate service developments ultimately influence the resilience of society to rising climate hazards^{1,2}. The spatial resolution of global climate models (GCMs) and the representation of physical processes and interactions have improved considerably since the 1950s, and the latest IPCC report (AR6) builds on a new set of climate projections from the Coupled Model Inter-comparison Project Phase 6 (CMIP6; ref. 3). Nevertheless, many small-scale features and phenomena such as, e.g., highly variable topography or organized convection, remain unresolved in most GCM simulations⁴. Dynamical downscaling, that is, running a regional climate model (RCM) for a limited domain with coarser GCM data at the boundaries, has been established as an important modeling branch as it entails more realistic regional climate representations⁵, although the benefits depend on the variable and domain of interest^{6–9}. The first multi-model RCM experiments at convection-permitting km-scale resolution are already available^{7–9}, yet such simulations are typically only performed for short periods (e.g., refs. 7–9) due to the immense computational demands. As such, RCM simulations that serve as the foundation of climate services in different countries (e.g., for Belgium¹⁰, the UK¹¹, Switzerland¹², or Germany¹³) generally have a resolution of ~ 10 km or coarser. While RCMs were not widely used for the IPCC AR5 (ref. 14) as worldwide coordinated intercomparison studies were still

emerging, in the IPCC AR6, RCMs from the Coordinated Regional Downscaling Experiment (CORDEX; refs. 15–17) provide the basis for sub-continental climate information (e.g., Chapters 11, 12 and Atlas, refs. 18–20).

Europe has warmed faster than any other World Meteorological Organization region since the 1980s, with annual mean temperatures increasing twice as much as the global average²¹. This is even more pronounced in Western Europe, where temperatures increase nearly three times faster than the global average (~ 2.3 °C compared to ~ 0.8 °C according to reanalysis, as shown later). Most CORDEX models, however, strongly underestimate the warming in Europe, especially during summer (Section 22–24). CMIP6 GCM simulations also tend to underestimate the warming in Europe compared to observations²⁵, although the warming discrepancy is less pronounced. Considering that climate services strongly rely on climate models, it is paramount to understand the causes of this inconsistency. If the models do not adequately represent the processes underlying the observed regional warming, this likely also affects climate projections. It is thus helpful to partition the signal into contributions from different physical drivers of rising temperatures: Regional warming is the consequence of (i) the background global warming, (ii) large-scale circulation changes, often conceptualized as dynamics, and (iii), regional changes in the surface energy budget and partitioning, including snow/ice–albedo–temperature and soil

moisture/vegetation–temperature feedbacks (thermodynamics). We note here that the (projected) near-surface summer temperature rise is constrained by the vertical warming structure, which enables enhanced near-surface warming over most extratropical land areas due to moisture limitations²⁶. Human-induced increases in greenhouse gas (GHG) concentrations strengthen the downwelling longwave radiation and thereby increase the surface net radiation, both initiating global warming and inducing a local thermodynamic forcing for a region of interest. In the case of Europe, an additional anthropogenic forcing is relevant: decreasing aerosol emissions have significantly reduced the attenuation of incoming surface shortwave radiation since about 1980 (e.g., refs. 27,28). Note that the global climate effect of aerosols depends on whether they absorb (primarily black carbon) or scatter (e.g., sulfate) radiation, resulting in a warming or cooling effect. However, increases or decreases in aerosol concentrations always invoke cooling or warming of the local near-surface climate, respectively, regardless of their global effects²⁹. Anthropogenic changes in radiation due to decreasing aerosol emissions have exacerbated the warming in mainland Europe since the 1980s, with shortwave forcing from direct aerosol effects being the primary driver of the surface energy budget²⁷, although a reduction in clouds could also have played a role³⁰. The CORDEX multimodel mean has, however, been found to underestimate the observed increase in downward shortwave radiation³¹, since most RCMs do not consider time-evolving aerosols³². Based on GCM climate projections featuring further declining aerosol emissions in the future, neglecting long-term changes in aerosol concentrations in regional EURO-CORDEX simulations causes an underestimation of the mean summer warming at the end of the current century by 1.5 to 2 °C for most of Europe³³. Therefore, as first suggested by an analysis based on a single RCM for the Euro-Mediterranean domain³⁴, different aerosol representations in CORDEX simulations might also contribute to the 1980–2022 warming discrepancy with respect to observations, which we aim to analyze further in this study.

Both the background warming and local thermodynamic forcing arise primarily in response to anthropogenic emissions, with globally increasing GHG and decreasing aerosol concentrations over Europe (and other regions). Regional warming can also occur naturally, however, as the atmosphere displays abundant internal variability at all timescales, generated both within the atmosphere and through interactions with slower components of the climate system such as the ocean. The North Atlantic Oscillation (NAO) and Atlantic Multidecadal Oscillation (AMO), e.g., are known to modulate the climate across much of the northern extratropics^{35–37}, and have contributed to rising air temperatures in the Northern Hemisphere, especially in the late 1990s and early 2000s (ref. 38). Recently, circulation changes have been linked to accelerated heatwave trends in Western Europe, but it remains unclear whether these dynamical changes are the result of natural climate variability or constitute a response to the human-induced climate warming³⁹. Thus far, externally forced changes in the atmospheric circulation have generally been considered “fairly small” compared to unforced internal variability^{40,41}, in agreement with analyses of large initial condition Earth System Model (ESM) ensembles^{42,43}. Either way, if the simulated dynamical changes are not in line with observations, this could cause a warming discrepancy. In fact, a study has suggested that a weaker dynamical contribution in CMIP6 simulations compared to observation-derived data could be the main cause of an underestimation in the simulated rise in heat extremes⁴⁴. This could imply that the warming mismatch is at least partly caused by long-term changes or inter-decadal variability in atmospheric dynamics not captured by climate model simulations, although the impact on summer mean temperatures has not yet been quantified.

This study focuses on summer warming in Western Europe from 1980 to 2022. We analyze both observation-derived and climate model data to estimate the thermodynamic and dynamic contributions to this warming. Additionally, we identify the causes for the climate model underestimation of mean warming over this highly populated region. We find two main factors that cause lower than observed regional

temperature increases: both multi-model ensembles yield a smaller dynamical contribution than observation-derived data, leading to an underestimation of the observed trend by about 0.6 °C (CMIP6 GCMs) and 0.8 °C (CORDEX RCMs). This is partially compensated by excessive background warming in both ensembles (>0.3 °C). However, the CORDEX RCMs further display a lack of regional thermodynamic warming. This warming mismatch on the order of 0.5 °C is primarily caused by omitted changes in aerosol forcing in a majority of the participating RCMs, and largely accounts for the underestimation of the CORDEX ensemble-mean thermodynamic warming. This regional thermodynamic bias in RCM simulations is of high relevance for country-level climate services, which tend to rely on these simulations in Europe due to their higher resolution.

Results and discussion

Comparing simulated and observation-derived warming in Europe

Since 1980, much of Europe has warmed by more than 2 °C during summertime (June–August), with some areas even exceeding a warming of 3 °C in ERA5 (Fig. 1a), resulting in an almost three times larger regional warming compared to the observed global warming over that time frame (0.8 °C). Based on a state-of-the-art 49-member RCM simulation ensemble from the CORDEX EUR-11 experiment at 0.11° or about 12.5 km horizontal resolution, however, the modeled warming signal is far weaker (blue colors in Fig. 1b). Averaged over the land areas of western West-Central Europe (WWCE; delineated in Fig. 1a, b) and gauged with linear trends, this amounts to 1.0 °C less warming than observed (ERA5, 2.3 °C). We focus our analysis on the WWCE region and provide area-averaged summer temperatures; all timeseries are smoothed and expressed as changes with respect to 1980 (see Methods for details). We note that this entails no assumption of linearity, and hence the resulting long-term temperature changes visualized in Fig. 1c are generally similar – but not identical—to linear trends. Only a few CORDEX simulations feature a warming of more than 2 °C since 1980 (purple range in Fig. 1c), and even the simulation with the strongest temperature increase (thin purple line) only slightly exceeds the warming in the ERA5 reanalysis. This suggests that there is a systematic bias in either (a) the prescribed forcing, (b) the regional model response to this forcing, or (c), a strong misrepresentation of the variability. The CMIP6 multi-model ensemble (green shading in Fig. 1d) also features weaker than observed trends in most simulations. However, the upper bound of the CMIP6 warming range is considerably higher compared to CORDEX, and the overall distribution actually includes the ERA5 data, thus not necessarily implying a discrepancy. We remark here that we do not expect a perfect correspondence between WWCE warming in CMIP5 GCM-driven RCM simulations and CMIP6 GCMs, for example because the latter employ a longer historical period in CMIP6 compared to CMIP5 (up to 2014 rather than 2005) and different aerosol and greenhouse gas emission scenarios thereafter. Nevertheless, this does not explain the widespread lack of WWCE warming in CORDEX simulations, which also feature less warming in winter and spring than observation-derived datasets, whereas linear trends in simulated and observed fall temperature are fairly consistent (Fig. 1e). Our analysis focuses on summertime temperatures, because compared to other seasons, (i) summer has warmed the fastest since 1980 according to both ERA5 and E-OBS (Fig. 1e), and (ii), elevated summer baseline temperatures fuel more intense and frequent heatwaves that exert greater impacts on society and ecosystems (e.g., refs. 4,45).

Revisiting the drivers of regional warming, we first examine whether insufficient background warming contributes to the summer warming discrepancy in WWCE. The background warming is indicated by linear trends in global annual mean 2m-temperatures from the corresponding driving GCM of each CORDEX simulation, and visualized together with WWCE summer warming since 1980 (purple dots in Fig. 2a). Ideally, we would find most model simulations near ERA5

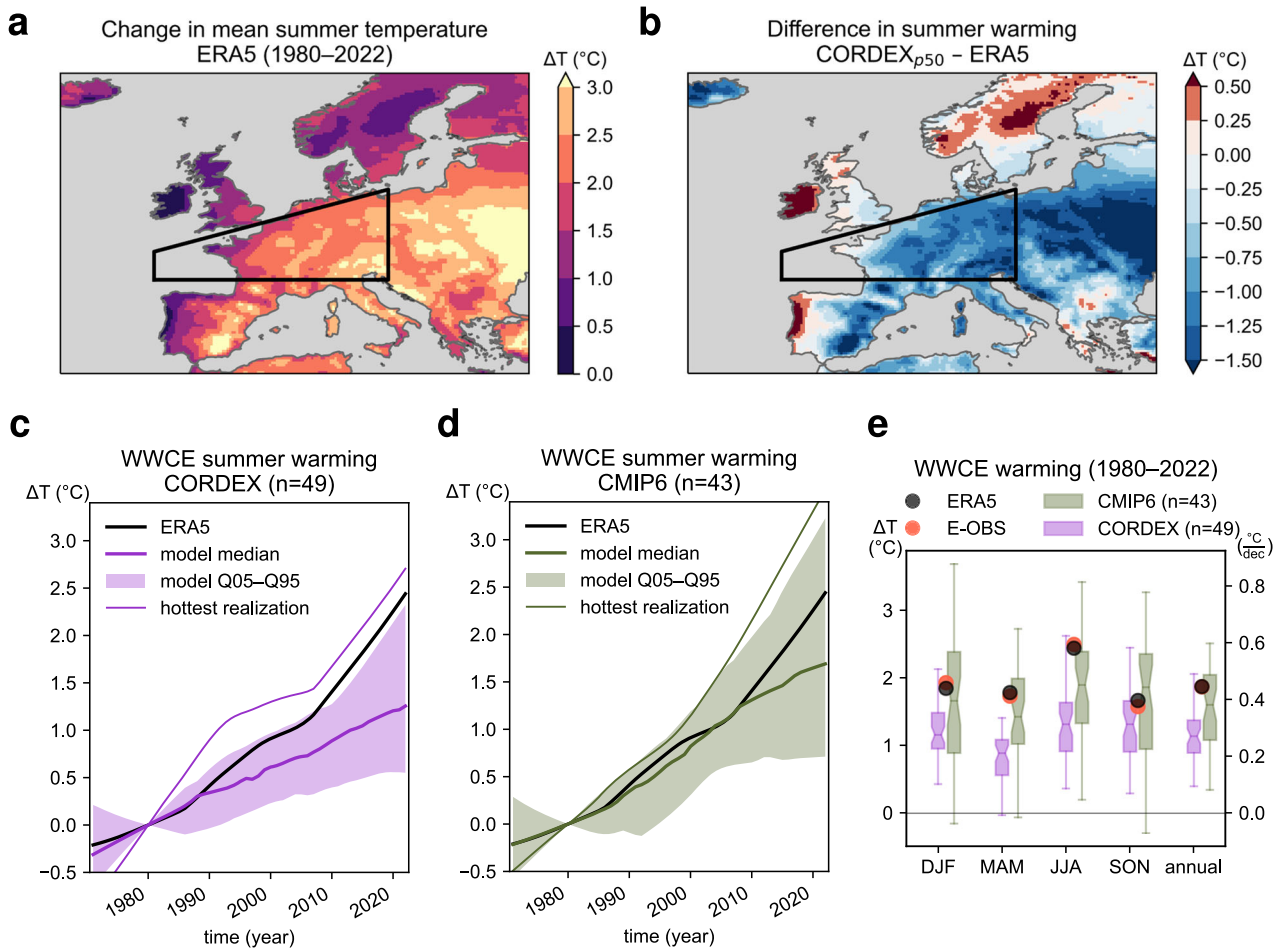


Fig. 1 | Summer warming in Europe underestimated by global and regional climate simulations. **a** Total change in summer mean 2m-temperature (1980–2022) estimated from a linear regression for ERA5, and **(b)**, the difference of the median warming obtained for a 49-member CORDEX ensemble and ERA5. In both **(a, b)**, the analysis region—the western half of West–Central Europe (WWCE)—is delineated by a black contour. Calculated using all land areas within this domain, **(c, d)** depict smoothed regional average summer temperatures, comparing ERA5 (black line) to CORDEX and CMIP6 simulations (colored range and lines), respectively. All

timeseries are represented by 31-year moving regressions to suppress high-frequency variability, and indicate changes with respect to 1980 (detailed in Methods). **e** 1980–2022 seasonal and annual mean warming estimated with a linear regression, using model data (purple: CORDEX RCMs, green: CMIP6 GCMs), reanalysis (ERA5, dark gray) and gridded observations (E-OBS, red). The center line, box, and whiskers of each boxplot indicate the median, the upper and lower quartiles, and the 1.5x interquartile range, and dots correspond to outliers.

(black marker) with respect to both dimensions, i.e., the background global warming as well as the WWCE summer temperature rise. The CORDEX ensemble used here is forced by 8 individual GCMs, that is, there are only 8 independent realizations of background global warming. Most of these GCMs clearly exceed ERA5’s 1980–2022 global mean temperature increase of 0.8 °C. A majority of CMIP6 simulations also overestimate the global mean temperature change compared to ERA5, but the range of background warming is substantially larger than for the CORDEX ensemble. Still, most regional temperature increases of ~1 °C or less are found in CORDEX simulations, and nearly all of these also remain below the 1:1 line, i.e., they feature less WWCE summer warming than for the entire globe throughout 1980–2022. At the other end of the simulated regional warming spectrum by the CORDEX ensemble, a handful of models manage to reproduce ERA5-like WWCE warming, but at a staggering background global warming of ~1.6 °C, i.e., double the observed global warming. Similarly, CMIP6 models associated with strong WWCE warming generally feature stronger than observed global mean temperature changes. These simulations agree with the observed WWCE summer warming for the wrong reason, since climate models should accurately capture the regional response to global warming (rather than to underestimate this response but simultaneously overestimate the warming at global scale).

Unraveling dynamic and regional thermodynamic warming contributions

Therefore, we continue our analysis for a subset of simulations with the most accurate background global warming compared to ERA5 (indicated by black marker edges in Fig. 2a). We find that differences in WWCE warming between simulations and the reanalysis product emerge more clearly (Fig. 2b), particularly for the CORDEX model subset. Inspecting the temporal evolution of surface net radiation for the same simulation subsets and domain (Fig. 2c), ERA5 points to a strong increase, whereas most—but not all—CORDEX simulations indicate only weak net radiation changes. This implies that most of the CORDEX ensemble members suffer from a bias in the regional thermodynamically induced trend. We examine this more closely further below, but already note that this is caused by different aerosol representations in the RCMs within CORDEX³². In contrast, the CMIP6 subset used here shows no clear forcing bias. Nonetheless, the strong-observation-derived temperature rise is still not captured (cf. model median vs. ERA5 in Fig. 2c). This suggests that the sole remaining regional warming driver—atmospheric dynamics—contributes to deviating temperature trends.

In a next step, we thus disentangle the 1980–2022 summer warming in WWCE into a dynamic and a thermodynamic component using dynamical adjustment for ERA5 and climate model simulations (see Methods).

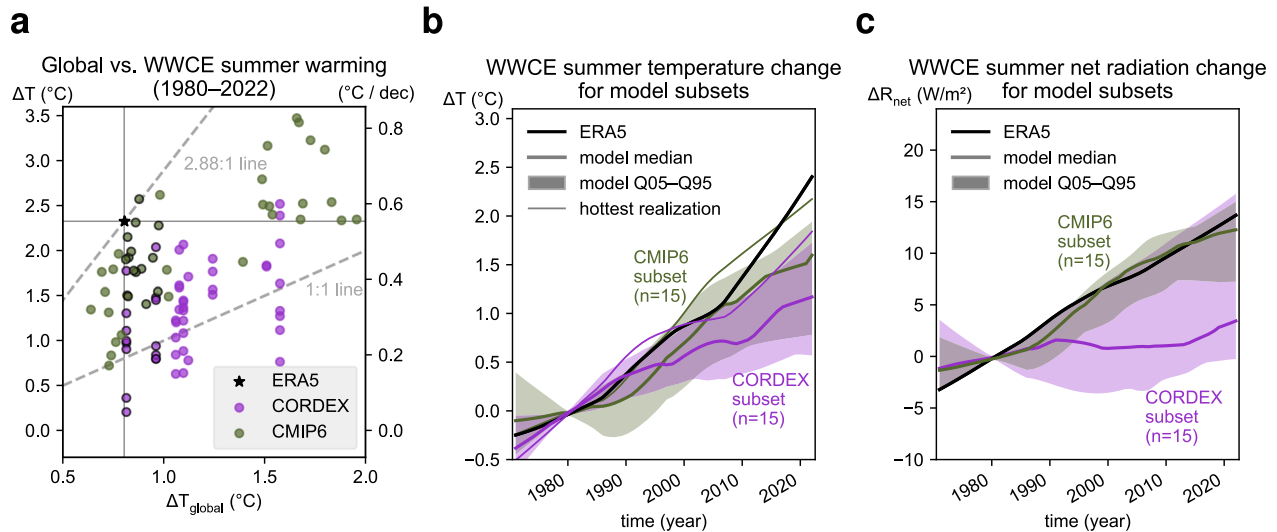


Fig. 2 | Simulations with near-actual background global warming largely underestimate the concurrent WWCE summer temperature increase. **a** Linear trends in WWCE JJA temperature and background global warming for 1980–2022 in ERA5 (black star), CORDEX and CMIP6 simulations (purple and green dots, respectively). CORDEX simulations driven by the two GCMs with global warming rates closest to ERA5 have black edges ($n = 15$; on average about $0.9\text{ }^{\circ}\text{C}$ as compared

to $0.8\text{ }^{\circ}\text{C}$ for ERA5). Similarly, the same number of CMIP6 experiments most consistent with this background warming is selected for further analysis, and the corresponding simulations are marked. **b** WWCE summer temperature for ERA5, CORDEX and CMIP6 simulations as in Fig. 1c, d, but restricted to the model subsets highlighted in a, with black dots. **c** As (b), but showing the summer mean surface net radiation for WWCE.

With this approach, we first estimate the impact of large-scale circulation changes over Europe—represented with 500-hPa geopotential height fields—on mean WWCE summer temperatures, i.e., the dynamical contribution to the total regional warming (schematically represented in Fig. 3a). The thermodynamic contribution is then obtained as the residual, and corresponds to the combined effects of the warming that is achieved within WWCE, mostly in response to increasing net radiation but possibly aided by soil drying, and beyond the region itself (conceptualized here as background global warming). Figure 3b visualizes total summer warming over 1980–2022 for model simulations, again for subsets of the CORDEX and CMIP6 ensembles constrained by background warming, and ERA5. For the latter, circulation increases the regional temperature change by $0.74\text{ }^{\circ}\text{C}$, which is nearly one third of the total warming (Fig. 3c). Most CMIP6 simulations feature positive, but generally far weaker dynamic contributions, leading to an underestimation of the temperature increase. These findings are consistent with a recent study that suggests dynamics as the main culprit for discrepancies between observed and simulated trends in heat extremes⁴⁴. Given that dynamic warming in GCM simulations is primarily an expression of (unforced) internal variability rather than externally forced^{42,43}, dynamically inflicted differences between ensemble mean and observed temperature trends do not imply systematic model biases.

Still, a clear majority of the CORDEX simulations features slightly negative dynamical contributions to the summer warming, which causes an even stronger underestimation of the temperature trend. The difference in dynamical contributions between these model ensemble subsets should be interpreted with caution; the 15 RCM simulations used here are driven by 2 GCM simulations that largely prescribe the large-scale atmospheric flow within the respective RCM domain boundaries⁴⁶, such that there are effectively only 2 independent circulation realizations. The 15 GCM simulations that form the CMIP6 subset, on the other hand, all feature a freely evolving global atmosphere and ocean, which explains why the range is wider than for the CORDEX RCMs. This also holds for the entire (unconstrained) model ensembles (Supplementary Fig. 1), and although the overall difference between simulated dynamical warming is smaller than for the subsets shown in Fig. 3c, the CORDEX models still largely feature negative (ensemble mean $-0.05\text{ }^{\circ}\text{C}$) and hence even weaker contributions than the CMIP6 ensemble ($+0.20\text{ }^{\circ}\text{C}$ on average). This does not explain the entire discrepancy with respect to the observed warming, however, since the

CMIP6 and CORDEX subsets also underestimate the thermodynamic warming (Fig. 3d) by -0.12 and $-0.38\text{ }^{\circ}\text{C}$ on average.

The strong thermodynamic bias apparent for the CORDEX models, being driven by simulations with nearly identical background global warming as across the CMIP6 subset (markers with black dots in Fig. 2a), must have a regional origin. More available surface net radiation enhances the surface turbulent heat fluxes, which is known to (i) directly impact air temperatures through surface sensible heating, and (ii), further enhance the net radiation through surface latent heating by the associated moistening of the atmosphere and resulting water-vapor feedback²⁷. We thus relate the thermodynamic warming to changes in the surface net radiation in WWCE. A relatively linear relationship emerges (markers and fitted green line in Fig. 4a), with a temperature sensitivity of about $0.5\text{ }^{\circ}\text{C}$ for a 10 W/m^2 net radiation change in line with earlier estimates⁴⁷. Following the aerosol representation classification of ref. 29, the CORDEX models with constant aerosols feature weak, mostly positive surface net radiation trends (red markers in Fig. 4a). The remaining CORDEX simulations with time-evolving aerosols, on the other hand, exhibit net radiation increases broadly consistent with ERA5 (blue markers in Fig. 4a). A budget analysis performed for ERA5 and all available simulations—regardless of background warming—reveals that changes in WWCE surface net radiation are predominantly fuelled by enhanced downward shortwave radiation, and to a lesser extent downward longwave radiation (Fig. 4b), as previously reported²⁷. This does, of course, not hold for the CORDEX simulations that (by design) neglect long-term decreases in aerosol concentrations over Europe since the 1980s, resulting in a comparatively minuscule shortwave forcing as reported previously (e.g., ref. 31).

The striking discrepancy of shortwave forcing in CORDEX simulations with and without time-evolving aerosols implies that the downward shortwave radiation increase evident for ERA5 and CMIP6 is largely caused by temporally evolving aerosol attenuation. Additional analyses presented in the Supplementary Information confirm that cloud-related shortwave radiation changes are minor ($+1\text{ W/m}^2$) compared to aerosol effects ($+21.3\text{ W/m}^2$) for ERA5 (Supplementary Fig. 2a). This is in line with evidence for decadal variations in observed shortwave radiation since the mid-20th century in West-Central Europe being primarily human-induced²⁸ (rather than, e.g., caused by changes in cloudiness). While CMIP6 models tend to have stronger cloud contributions than ERA5, aerosols remain the

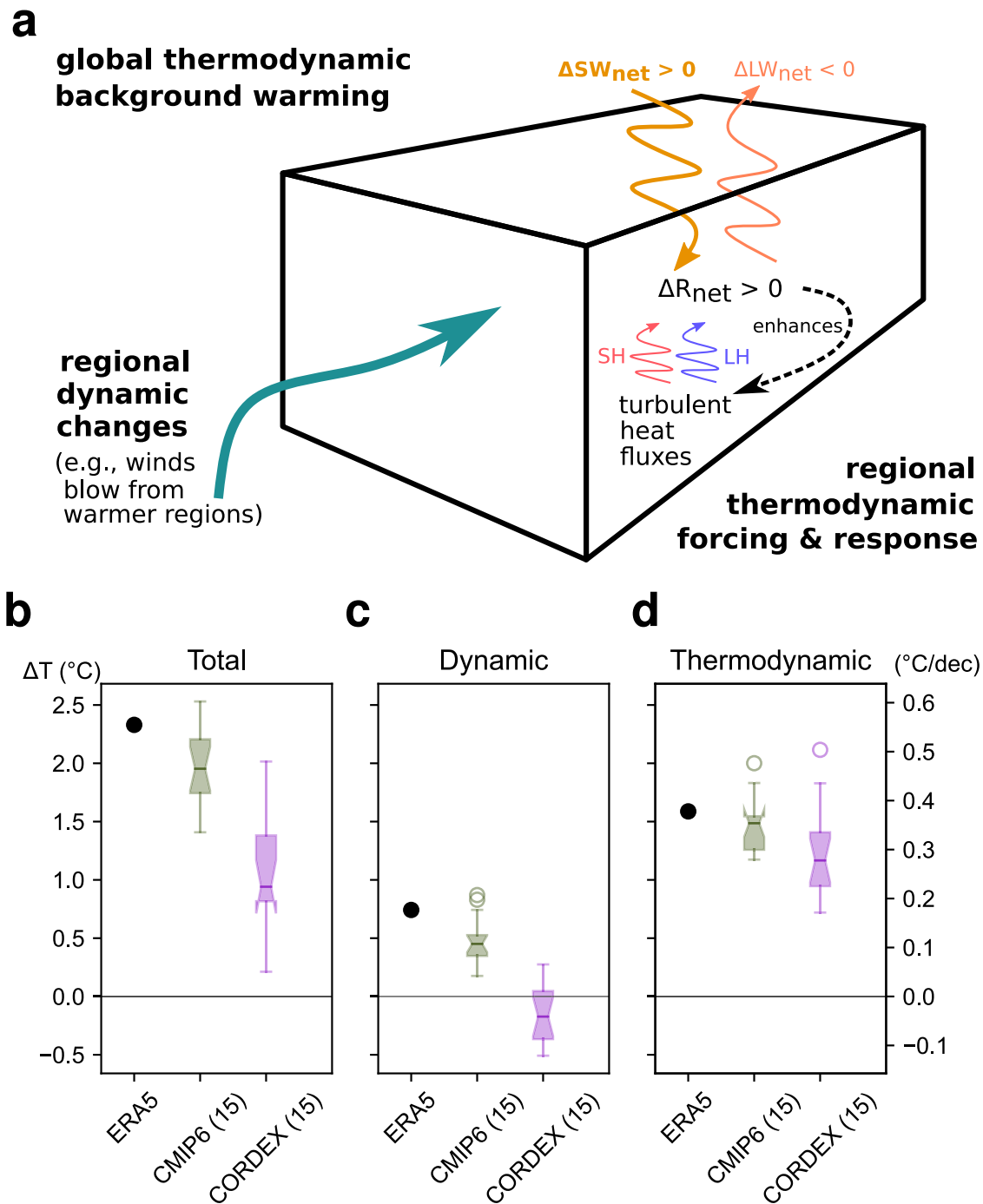


Fig. 3 | Disentangling the dynamic and thermodynamic drivers of summertime warming in WWCE. **a** Schematic representation of our analysis region, western West-Central Europe, and the drivers of regional warming, depicting: the (human-induced) global mean temperature increase that provides a ‘background’ warming to the region, the presence of a regional thermodynamic forcing (primarily due to increasing net radiation) and the resulting warming response, and dynamic changes. Note that this schematic focuses on the direct physical drivers of regional warming, which can in turn be affected by other processes and interactions; e.g., land cover changes may affect the surface energy partitioning and/or the surface albedo and hence ΔSW_{net} , and aerosols primarily modulate the attenuation of shortwave

radiation (and hence also ΔSW_{net}). **b** Total 1980–2022 summer warming for the RCM and GCM subsets from Fig. 2 with near-observed background warming, and ERA5 (black marker). The warming is gauged with linear trends and expressed as temperature change across the whole period, and per decade (secondary vertical axis). **c** Dynamic contribution to the WWCE summer temperature trend. **d** Total thermodynamic contribution to the WWCE summer temperature trend, enabled by both background global warming and regional thermodynamic forcing. The center line, box, and whiskers of each boxplot indicate the median, the upper and lower quartiles, and the 1.5x interquartile range, and dots correspond to outliers.

key driver of increasing shortwave radiation (Supplementary Fig. 2b). This further substantiates that neglecting time-evolving aerosols causes a lack of regional thermodynamic forcing and resulting warming response. As an additional line of evidence, we also examined CORDEX RCM simulations driven by ERA-Interim, the predecessor of ERA5, and found that all RCMs

with constant aerosols except for RegCM4-6 underestimate the WWCE summer warming compared to ERA-Interim itself (Supplementary Fig. 3). Before we proceed with our analysis for WWCE, we note here that European aerosol concentrations are largely attributable to local to regional emissions, which are highest in eastern and southeastern parts of the

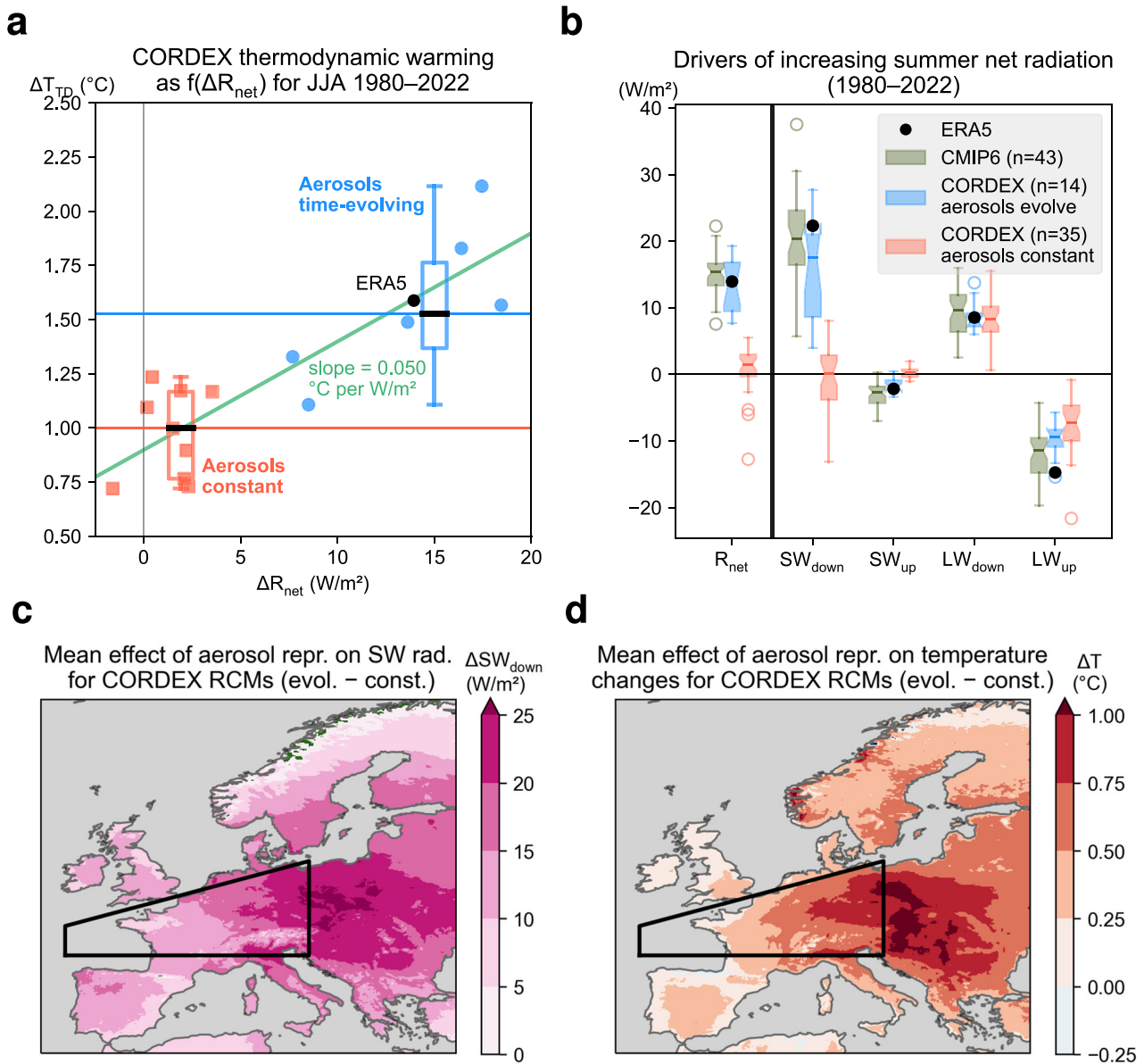


Fig. 4 | Constant aerosol forcing in CORDEX RCM simulations leads to underestimated net radiation increases, introducing a thermodynamic warming bias. **a** Changes in net radiation and thermodynamic warming in WWCE for the 15 CORDEX simulations driven by the 2 GCMs whose global warming rates are closest to ERA5 (as in Fig. 2c, d). The markers indicate whether the respective RCM includes time-evolving or constant/no aerosols (blue dots and red squares, respectively). **b** Changes in net radiation and its drivers for reanalysis and model

data, again grouping CORDEX simulations according to aerosol representation. **c** Mean difference in 1980–2022 downward shortwave radiation trends between the two subgroups by aerosol representation from (a), indicating the impact of long-term aerosol emission reductions compared to RCM simulations with temporally constant aerosol forcing. **d** As (c), but for near-surface temperature trends. The center line, box, and whiskers of each boxplot indicate the median, the upper and lower quartiles, and the 1.5x interquartile range, and dots correspond to outliers.

continent⁴⁸. What is more relevant for our analysis, however, is that aerosol emissions have declined faster and from a higher level in the east than any other part of Europe since 1980 (ref. 48). Consequently, at the eastern edge of our analysis region, and particularly even further to the east, downward shortwave trends for 1980–2022 are underestimated more severely in simulations with constant aerosol forcing than in any other part of Europe (Fig. 4c). This finding is corroborated by ERA5 downward shortwave radiation trends, which also depict stronger increases towards the east, as well as in-situ measurements that reveal the same east–west gradient (Supplementary Fig. 4). In terms of the impact on temperature trends, our analysis region is more affected than southern or northern Europe (Fig. 4d), but even stronger differences emerge to the east with local exceedances of 1 °C, consistent with the pattern in shortwave trend biases (Fig. 4c) and aerosol emissions⁴⁸.

Quantifying the aerosol forcing-induced warming mismatch

Building on the disentangled warming contributions from the dynamical adjustment, we estimate the warming mismatch caused by neglecting long-term changes in aerosol concentrations. Starting with our RCM subset driven by the two CMIP5 GCMs with reasonable 1980–2022 global warming, we obtain a thermodynamic WWCE summer warming of about 1.0 and 1.6 °C for constant and evolving aerosol representations, respectively, with the latter being close to ERA5 (Table 1). Therefore, for this model subset, the aerosol effect amounts to about 0.6 °C, and this also holds when the total temperature changes are directly compared to one another as the dynamic contributions are identical (–0.16 °C). This estimate is, however, dependent on the GCM–RCM model chains that are part of the subset; for the entire ensemble, the estimated aerosol effect only amounts to 0.35 °C. Taking into account that the simulations with constant aerosols are driven

Table 1 | Summer warming in WWCE between 1980 and 2022 for CORDEX RCM simulations and ERA5, disentangled into dynamic and thermodynamic contributions (see Methods)

	Total warming	Dynamic warming	Thermodynamic warming (regional + background)	Global background warming	Estimated aerosol effect
ERA5	2.33	0.74	1.59	0.81	/
CORDEX subset, aerosols evolving	1.42	-0.16	1.57	0.89	-0.60
CORDEX subset aerosols constant	0.83	-0.16	0.98	0.88	
CORDEX all, aerosols evolving	1.55	-0.07	1.62	1.08	-0.34 (*)
CORDEX all, aerosols constant	1.24	-0.04	1.28	1.16	

We also show the global background warming that contributes to the total thermodynamic warming, and provide an estimate of the aerosol effect based on the difference in thermodynamic warming between RCMs with evolving and constant aerosols. This estimate does not take the underlying background warming into account, which is consistent across the subset yet higher for the subgroup with constant aerosols in the entire ensemble (*). We do this both for the RCM subset with near-ERA5 background warming and the entire ensemble, which yields two distinct estimates (see also discussion in the main text). Any warming is estimated with a linear trend, and represents the respective total 1980–2022 changes. All values are shown in °C. We present separate results for each of the 49 CORDEX GCM–RCM model chains in Supplementary Table 1.

by GCMs with slightly higher background global warming than those with time-evolving aerosols (1.16 vs. 1.08 °C), the actual aerosol-related warming across the whole ensemble is likely larger than 0.4 °C.

In a next step, we return to Fig. 4a where net radiation changes are related to thermodynamic warming, but instead group simulations by the same driving GCMs (Supplementary Fig. 5). There are three RCMs with evolving aerosols, and two of those simulate clearly stronger warming than the third RCM. Repeating the calculation of aerosol-related warming contributions separately for each of these three RCMs, we find aerosol effects near 0.5 °C or higher for ALADIN63 and HadREM3, yet comparatively minuscule effects for RACMO22E (around 0.1 °C) based on both our model subset and the whole ensemble. Since RACMO22E has a larger share of the total evolving aerosol simulations for our full GCM–RCM ensemble, this partly explains why we find weaker aerosol-related temperature effects than for the subset. It is difficult to assess whether HadREM3 and ALADIN63 should be considered as more indicative of the ‘actual’ aerosol-related warming, because in all cases, the reference merely consists of other RCM simulations with constant aerosols and potentially different model errors. An ideal comparison would be based on simulations with constant and evolving aerosols for each RCM. We cannot offer such a comparison here, but consider an aerosol-related summer warming of about 0.5 °C or higher across 1980–2022 in WWCE reasonable in light of the presented analysis. In relative terms, the global background warming amounts to about half (ERA5) or more (CORDEX RCM simulations) of the total thermodynamic warming, and at least one third is caused by declining aerosol concentrations within Europe.

We emphasize that our analysis region does not include the areas with the strongest aerosol-related warming, as the estimated effect peaks east of WWCE. We hence repeated the disentangling of summer warming into dynamic and thermodynamic contributions based on ERA5 for eastern West-Central Europe (EWCE; displayed in Supplementary Fig. 6), and found that dynamic contributions are nearly identical to WWCE, whereas the thermodynamic warming is clearly higher (2.0 °C as opposed to 1.6 °C; Supplementary Fig. 7). We note here that even CORDEX simulations with constant aerosols point to slightly higher warming in EWCE than WWCE, which might reflect a weaker oceanic influence in the eastern half of WCE, and implies that the thermodynamic warming difference between east and west evident for ERA5 should not be entirely attributed to the difference in aerosol-related warming. Still, according to the CORDEX simulations with evolving aerosols, and whether based on the subset (Supplementary Fig. 7) or the full ensemble (Supplementary Fig. 8), aerosol effects are about 0.15 °C stronger in EWCE than WWCE. Although these estimates are based on total temperature changes rather than thermodynamic warming, we conclude that even faster warming due to aerosol changes in eastern parts of West-Central Europe might cause (and at least contribute to) the east–west gradient in model–reanalysis warming discrepancies evident in Fig. 1b.

Summarizing our analysis thus far, and despite potential inaccuracies due to comparing RCM subgroups with potentially different model errors, we have conclusively demonstrated that the thermodynamic warming underestimation by the CORDEX ensemble is largely attributable to aerosol representations. To our knowledge, previous analyses either examined the impact of aerosol representation in multi-model CORDEX ensembles on past (and projected) shortwave radiation changes^{31,32}, or investigated the influence on temperature in climate projections^{33,49}. Besides these studies, model experiments with a single RCM suggest that nearly a quarter of the simulated 1980–2012 annual mean warming in Europe is due to declining aerosol concentrations³⁴. Recently, a set of experiments based on a specific GCM–RCM pair was presented that can share the same grid and utilize identical model physics and forcings, designed to pinpoint the causes behind discrepancies in RCM and GCM simulations⁵⁰. It was found that different aerosol representations in RCMs strongly affect shortwave radiation and temperature projections, with the same east–west gradient across Europe emerging as in our analysis (cf. their Supplementary Fig. 10) and similar

results despite obvious methodological differences. Overall, our results suggest that the summertime warming in WWCE in RCMs without time-evolving aerosols—the majority of models participating in the CORDEX initiative—is largely driven by the background global warming, as the regional thermodynamic forcing and resulting warming is widely underestimated.

On the other hand, the RCMs with long-term aerosol changes simulate almost the same thermodynamic warming as obtained from ERA5 (cf. dashed lines in Fig. 5a). While these models reach the observation-derived 1980–2022 temperature change attributable to thermodynamics (yellow line in Fig. 5a) on average in the year 2026 (i.e., 4 years too late), it takes substantially longer for the simulations based on constant aerosols. As such, the RCMs with constant aerosol forcing only reach the current observed summer warming in an additional 13 years, despite being forced with a high-emission scenario. Note that under the RCP 8.5 emission scenario, emissions of major aerosol precursors across Europe generally decline further towards 2100. Crucially, the mismatch introduced by neglecting long-term aerosol changes relative to simulations that account for it thus increases throughout the ongoing century, reaching about 1.5 °C (and close to 2 °C) in terms of mean (median) in 2100 (cf. red and blue boxplots in Fig. 5a). This range is consistent with ref. 30, even though the authors employed a different CORDEX model ensemble. We emphasize that our estimates are based on subgroups consisting of RCMs with different model physics; for example, most RCMs do not consider plant physiological responses to rising CO₂ (i.e., closing stomata and hence reducing transpiration due to increased water use efficiency), which could lead to a general underestimation of the rise in future heat extremes⁵¹. ALADIN63 with time-evolving aerosols does represent physiological responses, however, which could distort our analysis, but on the other hand and for this specific RCM, physiological effects do not exert strong control on projected summer temperature changes in WWCE⁵⁰. Bearing the limitations of our analysis in mind, we repeat it for all seasons and find the strongest

aerosol representation effects on shortwave radiation changes and hence also temperatures in summer, followed by spring and autumn (~0.7 °C discrepancy in 2100), whereas no clear differences emerge for winter (Supplementary Figs. 9 and 10). This is precisely the result we would expect considering the strong seasonal cycle of downward shortwave radiation in a region such as WWCE, with comparatively weak insolation and short daytimes in winter⁵¹.

Thus far, we have explored how the lack of regional thermodynamic forcing due to neglecting decreasing aerosol concentrations affects summer mean temperatures. We now expand our analysis to different timescales, ranging from seasonal to daily (Fig. 5b). Unlike for the multi-model averages, the observation-derived 1980–2022 warming for the 5 hottest consecutive days outpaces both changes at shorter and longer timescales. We would not expect the latter if the warming was entirely driven by thermodynamics, and hence consider this an independent line of evidence that dynamics contributed to the summer warming in WWCE. Moreover, we note that the hottest sub-monthly periods occur most frequently in July and August for WWCE, whereas the observed monthly mean warming is clearly highest in June (Supplementary Fig. 11), fuelled by strong dynamic contributions. Consequently, discrepancies between ERA5 and CORDEX simulations also increase from 10/15-d periods towards the (90-d) seasonal scale. Comparing the mean warming rates of the two CORDEX subgroups, the hottest 10-d period per year increased by about 2 °C and 1 °C for CORDEX simulations with and without time-evolving aerosols, respectively, and the resulting ~1 °C difference implies an even stronger absolute thermodynamic contribution than for summer mean temperatures at ~0.6 °C. While the relative contribution to the total warming does not vary much as much across timescales, but tends to exceed 40%, it is not obvious why a long-term modulation of shortwave—and ultimately net—radiation trends by aerosols enhances temperatures during the hottest sub-monthly time periods more than across the entire summer. We argue that aerosol representation-inflicted biases should emerge most clearly in cloud-free conditions, which are closely related to the large-scale circulation patterns—typically atmospheric blockings—that enable heatwaves in WWCE (e.g.,

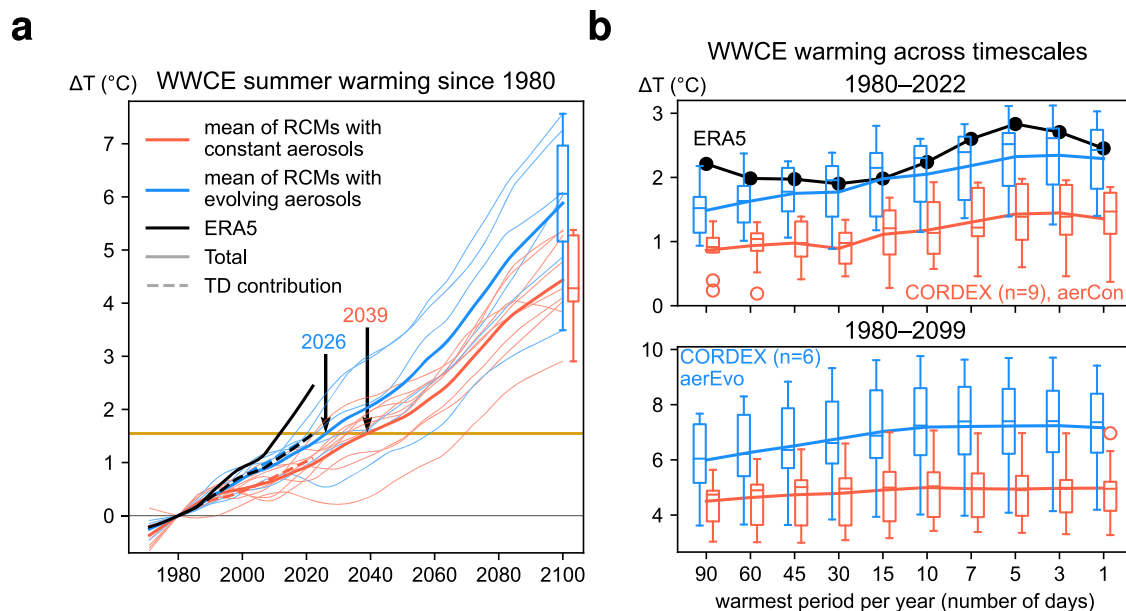


Fig. 5 | The thermodynamic bias inflicted by constant aerosol forcing increases throughout the ongoing century and emerges even more clearly at the timescale of heatwaves. a Long-term temperature changes since 1980 for ERA5 and the CORDEX subset, again grouped according to aerosol representation. Additionally, the thermodynamic warming obtained through dynamical adjustment is shown for the 1980–2022 period (dashed lines). The year in which ERA5’s current thermodynamic warming is reached by the respective ensemble means is also indicated. The

boxplots for both CORDEX model groups are calculated for the long-term change up to the year 2099. **b** Long term changes of the hottest n-day periods in each year between 1980–2022 and 1980–2099 in the upper and lower panel for ERA5 and the RCM simulations, determined by fitting a linear trend and calculating the total temperature change across the respective time period. The center line, box, and whiskers of each boxplot indicate the median, the upper and lower quartiles, and the 1.5x interquartile range, and dots correspond to outliers.

ref. 52). In fact, enhanced direct aerosol effects during blocking conditions in Europe have been linked both to reduced cloud cover and increased aerosol load⁵³.

Finally, repeating this analysis for 1980–2099 (bottom panel in Fig. 5b), we find aerosol-related temperature biases in excess of 2 °C for the hottest multi-day periods up to 15 days at the end of this century. This result is based on the assumption that by comparing the average simulated temperature changes of RCMs with and without evolving aerosols, we primarily delineate the impact of the aerosol representation rather than differences in dynamical contributions or model errors. Our analysis for summer mean warming suggests that on average, the dynamical contributions are nearly identical for RCMs with constant or evolving aerosols, yet it also indicates a somewhat unexpected model dependency with respect to both the net radiation and temperature impact of the ongoing decline in aerosol emissions over Europe since the 1980s. Our finding—the magnitude of future heatwaves in WWCE under a high (carbon) emission scenario is underestimated by more than 2 °C when neglecting regional anthropogenic aerosol effects—should thus be seen as a first estimate, and does not inform on differences between individual simulations but rather on the mean effect for our model subset. Bearing this in mind, we apply the same analysis to EWCE for which we already noted enhanced aerosol impacts on the mean summer warming compared to (western adjacent) WWCE. We find even stronger heatwave magnitude change discrepancies of nearly 3 °C between the subgroups with different aerosol representations (Supplementary Fig. 12), which is fully consistent considering the east–west gradients in both aerosol emission⁴⁸ and shortwave radiation changes. Owing to the clear physical link, that is, aerosol-driven changes in atmospheric attenuation of radiation affect the amount of energy available for the surface turbulent heat fluxes and hence the warming, we expect that the use of CORDEX RCM simulations with predominantly constant aerosols also leads to biases in simulated mean warming and heatwave magnitude changes in other regions of Europe and beyond. The effects in low-latitude, typically cloud-free areas could be even greater due to the strong insulation, although this also depends on the local aerosol concentrations as well as their future evolution.

Conclusion

In this study, we have shown that RCMs underestimate the past summer warming in Western Europe mainly for two reasons; (i) the dynamic contribution from circulation changes tends to be far weaker than suggested by the ERA5 reanalysis, and (ii), most CORDEX RCMs do not capture the local thermodynamic forcing by neglecting aerosol-mediated shortwave radiation changes. The circulation changes may well be a symptom of multi-decadal natural variability and hence be unforced. Thus, the dynamically inflicted warming discrepancy is not necessarily problematic. On the contrary, the thermodynamic biases introduced by keeping aerosol concentrations constant in the CORDEX simulations is of concern, not least because the associated warming discrepancies relative to models that account for time-evolving aerosols grow even larger in climate projections. The IPCC has emphasized that our confidence in RCM projections depends on whether the relevant processes, forcings (including aerosols) and drivers of climate change are adequately represented by the models⁵⁴. Our analysis demonstrates, however, that this does not apply to a majority of the RCMs used here. Because the CMIP5 driving GCMs portray a global background warming range with ERA5 at the lower end, the thermodynamic warming underestimation due to neglecting anthropogenic aerosol forcings is partly compensated, but not for the right reasons. This could be problematic if not taken into account by climate services that rely on these models, since complex and regionally diverse aerosol effects on climate should not be omitted when assessing future climate risks⁴⁹.

Compared to the RCMs that include long-term aerosol changes, the magnitude increase of heatwaves based on a high-emission scenario is underestimated by about 1 °C and 2 °C for 1980–2020 and 1980–2099, respectively. In Eastern Europe, where aerosol emissions have declined faster since the 1980s than further west, we not only find even stronger shortwave radiation increases, but also a more pronounced warming deficit for RCMs with constant aerosols reaching almost 3 °C for projected heatwaves at the end of the century. Such warming biases might distort the outcome of extreme event attribution analyses, since the probability of heatwaves tends to decrease strongly for increasing magnitude (e.g., ref. 55). Moreover, given that epidemiological studies suggest an exponential increase in heat-related mortality for the most extreme temperatures⁴⁵, it is crucial to estimate the future intensification of heatwaves due to human-induced climate change as accurately as possible. Only then can climate services provide reliable information to decision makers and stakeholders, and thereby contribute to adequate adaptation measures. In light of the upcoming next generation of CORDEX RCM experiments driven by CMIP6 GCMs, we provide two specific recommendations: First, the driving GCMs are selected based on several criteria including model performance, model independence and projected climate change diversity⁵⁶, but it might make sense to additionally consider the accuracy of historic thermodynamic warming patterns. Second, we recommend increased efforts to improve the aerosol representations in the RCMs, such that they at the very least include anthropogenic long-term changes in the direct aerosol effect. This would improve both the consistency of CORDEX simulations with respect to the driving CMIP6 GCMs and their ability to reliably depict historical and future climate change.

Methods

Analysis period and domain

Our main analysis is restricted to boreal summer (June–August) in 1980–2022 (or 1980–2099), and we focus on the western half (–10°W to 15°W) of West-Central Europe (WCE), an IPCC climate reference region⁵⁷, referred to WWCE hereafter. This choice is motivated by the fact that the eastern edge of the entire WCE region at 40°W is too close to the regional model domain boundaries to apply the dynamical adjustment approach described further below. The western corner coordinates of WWCE are identical to WCE (–10°W, 45 or 48°N, respectively), whereas the eastern corners are at 15°W and 45 or 54.65°N. All climate variables are area-weighted when calculating regional means, for which only terrestrial data is employed.

Observation-derived and in-situ data

The fifth-generation European Center for Medium-Range Weather Forecasts (ECMWF) atmospheric reanalysis of the global climate, ERA5, produces hourly records of the atmosphere, land surface and ocean waves by optimally merging numerical model output and observations^{58,59}. We use ERA5 as a reference for climate models and to estimate the dynamic and thermodynamic warming contributions, including 2-meter temperature, radiation and 500-hPa geopotential height data from 1950 to 2022 at a horizontal resolution of 0.25°.

ERA5 employs sulfate aerosol forcings from CMIP5 (ref. 58), in turn based on a reconstructed aerosol emission inventory⁶⁰ up to 2009, and thereafter using emission scenarios (specifically RCP2.6; ref. 61). In other words, long-term changes in anthropogenic aerosols are solely considered for the dominant species⁶¹ and to the author's knowledge, only direct aerosol effects are represented (i.e., the scattering and absorption of radiation). On the one hand, this implies that ERA5 does not represent the full complexity and associated impacts of anthropogenic aerosol emissions, but on the other hand, this simplifies our comparison to the CMIP5 GCM-driven RCM simulations, since none of the RCMs with evolving aerosols represents all indirect effects either (i.e., cloud albedo and interactions between aerosols and cloud microphysics).

Only grid cells that consist of at least 50% land are considered. This approach does not noticeably impact our analysis of WWCE averages, but can introduce slight inconsistencies in the vicinity of coastlines when comparing against re-gridded CORDEX simulations (Fig. 1b).

In addition to ERA5 data, we employ ensemble mean temperatures from E-OBS v27.0e on a $0.25^\circ \times 0.25^\circ$ grid, covering the 1950–2022 period⁶². The E-OBS dataset provides a 20-member ensemble of gridded daily meteorological observations across Europe. Note that station data used to grid the point observations are usually not homogenized (except for v19eHOM, but this version does not cover our entire analysis period), and the station density varies in time, which could affect trend analyses.

Finally, we also use monthly downward shortwave (or global) radiation, collected by the Global Energy Balance Archive (GEBA). The latter is an international data center for the worldwide measured energy fluxes at the Earth's surface, maintained at ETH Zurich⁶³. The mission of GEBA is to compile all accessible sources of worldwide measured energy fluxes at the Earth's surface in a central data archive. GEBA has continuously been expanded and updated, and to date contains around 700,000 monthly mean entries of 15 different surface energy balance components measured at more than 2000 locations around the world. Many of the historic records contained in GEBA extend over multiple decades.

We note that only few stations have no missing values since 1980, and there is currently no data beyond June 2021. We first calculate monthly anomalies across all available timeseries in Europe, which we then average over each summer, requiring at least 1 available month

per summer and excluding any stations where this criterion is not met. By doing so, we ensure that we only rely on measurements that cover every single summer in the 1980–2021 period, but retain more data than by enforcing no missing monthly values at all. This choice does not affect the outcome of the comparison to ERA5 data; either way, and despite the expected discrepancies when comparing individual GEBA station trends (at the point scale) to reanalysis output (0.25°), we obtain a few near-zero but predominantly clearly positive global radiation changes, and observe the strongest increases in eastern Europe (SFig. 4).

Model data

We employ regional and GCM simulations from the EURO-CORDEX^{16,17} and ReKliEs-De¹³ projects at 0.11° (EUR-11) and CMIP6 (ref. 64), respectively, listed in Tables 2–4. For the GCM–RCM model chains of EURO-CORDEX and ReKliEs-De, historical simulations supply data up to 2005, and the remaining years are based on the high-emission representative concentration pathway scenario (RCP8.5). The same applies to the CMIP5 simulations⁶⁵ used to drive the CORDEX simulations, from which we obtain global mean temperatures to estimate the background warming. Similarly, for CMIP6, we concatenate historical and high-emission shared socioeconomic pathway simulations (SSP5-8.5) at the beginning of 2015.

We also use CORDEX evaluation simulations driven by reanalysis instead of GCMs to provide an alternative assessment of whether the constant aerosol representations in a majority of the RCMs causes warming biases. The length of RCM simulations driven by ERA-Interim⁶⁶ varies strongly, hence we always use all available data rather than a common period and compare the smoothed temperature evolution of RCM simulations to ERA-Interim data itself.

Native model grids are used to calculate regional averages for all simulations with `regionmask`. To compare grid-cell based trends in model simulations and reanalysis, CORDEX variables are regridded to a regular $0.25^\circ \times 0.25^\circ$ grid. Temperature is regridded bilinearly, all other variables are processed with a conservative regridding algorithm using `xESMF`.

Trend estimation

All trends are determined with a linear regression, and total changes are obtained by multiplying the slope (°C/year) with the number of years between 1980 and 2022 (42 years). To additionally estimate and visualize long-term changes without any assumptions of linearity, we also apply a Locally Weighted Scatterplot Smoothing (LOWESS) algorithm using `statsmodels` with the smoothing width set to 31 years. To facilitate the comparison of temporally evolving climate variables from reanalysis data or

Table 2 | Driving GCMs of the RCMs used for analysis

ID	GCM (CMIP5)	Ensemble member(s)
1	CanESM2	r1i1p1
2	CNRM-CM5	r1i1p1
3	EC-EARTH	r1i1p1, r12i1p1
4	IPSL-CM5A-MR	r1i1p1
5	MIROC5	r1i1p1
6	HadGEM2-ES	r1i1p1
7	MPI-ESM-LR	r3i1p1
8	NorESM1-M	r1i1p1

GCMs with near-ERA5 1980–2022 background warming (see next subsection) are shown in bold font. That all these CMIP5 GCMs include a transient aerosol forcing, i.e., they capture long-term changes in anthropogenic aerosols (see, e.g., Table 1 in ref. 31).

Table 3 | CORDEX GCM–RCM model chains used for analysis, all based on a single GCM ensemble member (usually r1i1p1) as listed in Table 2

Institution	RCM	GCM (CMIP5)	<i>n</i>	Aerosol forcing
CLMcom	CCLM4-8-17	(1), (2) , (3_r12), (5), (6), (7), (8)	7	constant
CLMcom-ETH	COSMO-crCLIM-v1-1	(3), (6), (7)	3	constant
CNRM	ALADIN63	(2) , (6), (7), (8)	4	time-evolving
DMI	HIRHAM5	(2) , (3), (4), (6), (7), (8)	6	constant
GERICS	REMO2015	(1), (2) , (3_r12), (4), (5), (6), (7), (8)	8	constant
ICTP	RegCM4-6	(2) , (3_r12), (6), (7), (8)	5	constant
KNMI	RACMO22E	(2) , (3), (4), (6), (7), (8)	6	time-evolving
MOHC	HadREM3-GA7-05	(2) , (3_r12), (7), (8)	4	time-evolving
MPI-CSC	REMO2009	(7)	1	constant
SMHI	RCA4	(3), (4), (6), (7), (8)	5	constant

EC-EARTH driven RCMs are driven by r1i1p1 except for CCLM4-8-17, HadREM3-GA7-05, REMO2015 and RegCM4-6, for which r12i1p1 was used (also indicated in the GCM column below). The number of available GCM–RCM model chains as well as the RCM aerosol forcing is also provided.

Bold indicates that the corresponding model chain (or simply GCM) has near-ERA5 background warming.

observations and model simulations, we represent all data as changes with respect to 1980 after applying the smoothing algorithm. To ensure that observation-derived estimates and model output are treated consistently, we remove any data prior to 1971 (since several CORDEX simulations are only available from then) and after 2022 before applying the LOWESS filter. The latter, unlike the widely used moving average, provides smoothed data for the entire timeseries. The sole exception to this consists of Fig. 5, for which model data is used up to 2099 to calculate smoothed timeseries and linear trends.

Model subsets with near-ERA5 background warming

The RCMs that form our 49-member CORDEX ensemble are driven by 8 different CMIP5 GCMs, and consequently have varying degrees of background global warming. The same applies to the GCMs participating in CMIP6. To analyze only simulations with similar global mean temperature increases, we define subsets for both model ensembles; in practice, this is achieved by limiting the 1980–2022 background warming—obtained with linear regression—to 1 °C for all CORDEX simulations. This is fulfilled for 15 out of 49 ensemble members driven by two GCMs (CNRM-CM5 and NorESM1-M), and yields a mean background warming of 0.89 °C (Table 5). We then select the same number of CMIP6 simulations closest to this value to obtain a subset with comparable background warming (0.84 °C). Compared to the remaining simulations, both subsets feature background warming broadly consistent with each other and ERA5 (0.81 °C). Our results and conclusions are not sensitive to these choices.

Disentangling dynamic and thermodynamic contributions to regional warming

We implemented a dynamic adjustment approach^{43,67,68} to disentangle the dynamic and thermodynamic contributions to the notable warming trends observed over WWCE. This approach is widely used to attribute a proportion of the variability in the target variable (here, summer mean

temperature) to changes in atmospheric circulation, under the assumption that other factors remain constant.

Here, we leverage principles from statistical learning and implement a regularized ridge regression method to establish a physical relationship between the summer mean temperature and the geopotential height at 500 hPa (Z500). Our model is trained on detrended Z500 fields (on a 2.5° × 2.5° grid) and detrended regional mean summer temperatures from a 2070-year pre-industrial control simulation obtained from CESM2. We detrend Z500 by subtracting the daily Z500 average over the circulation domain [30°W–35°E, 22°N–72°N] from the daily Z500 at each grid cell and at each time step across the domain⁶⁹. This is done to remove the effect of thermal expansion of the troposphere primarily caused by anthropogenically forced global warming on Z500. Nonetheless, it is important to note that changes in atmospheric circulation are not solely influenced by natural variability. External forcing can also potentially contribute to shaping these circulation patterns, which in turn can have effects on near-surface temperatures.

Note that we train our model on pre-industrial control instead of transient climate simulations to avoid the possibility of the regression model erroneously learning from forced warming signals⁴³.

We employ the following equation to isolate the circulation-induced component of summer mean temperatures,

$$t_n = f(m_{n \times p}) \tag{1}$$

where t_n represents summer mean temperature, n is the number of years, m is a matrix of detrended Z500 with dimensions $n \times p$ (p is the number of grid cells within the circulation domain), and f denotes a regularized ridge regression model. During the training phase on the control run, a k -fold cross-validation scheme is employed to fine-tune the regression model and prevent overfitting. The temperatures predicted (\hat{t}) by this model represent the circulation-induced components, while the residuals ($\hat{t} - t$) capture the externally forced thermodynamic signal in summer mean temperatures.

Finally, we provide the fitted model with summer averages of WWCE temperatures and Z500 fields from ERA5 as well as the CORDEX RCM and CMIP6 GCM simulations to estimate the respective dynamical contributions to the regional warming. This approach of calibrating to a single (typically long pre-industrial control) simulation, and then applying the fitted model to other (transient) simulation ensembles and/or reanalysis data has been extensively tested⁶⁷. We also include 89 members covering the period 1850–2100 from the CESM2 Large Ensemble (CESM2-LE; ref. 70), each branched from the same pre-industrial control run as we employ to train the regression model, but with unique initial conditions. Since this ensemble is based on a single model, we do not consider it in our main analysis, but still display the results in SFig. 1.

Table 4 | CMIP6 simulations used for analysis

GCM	Number of ensemble members
MPI-ESM1-2-LR	15
NorESM2-LM	1
UKESM1-0-LL	5
MIROC-ES2L	10
GFDL-ESM4	1
CMCC-ESM2	1
CanESM5	10

GCMs with ensemble members that feature near-ERA5 1980–2022 background warming (see next subsection) are shown in bold font.

Table 5 | As Table 3, but only listing CORDEX GCM–RCM simulations with near-ERA5 global warming since 1980

Institution	GCM (CMIP5)	RCM	Aerosol forcing
CLMcom-ETH	CNRM-CM5, NorESM1-M	COSMO-crCLIM-v1-1	constant
CNRM	CNRM-CM5, NorESM1-M	ALADIN63	time-evolving
DMI	CNRM-CM5, NorESM1-M	HIRHAM5	constant
GERICS	CNRM-CM5, NorESM1-M	REMO2015	constant
ICTP	CNRM-CM5, NorESM1-M	RegCM4-6	constant
KNMI	CNRM-CM5, NorESM1-M	RACMO22E	time-evolving
MOHC	CNRM-CM5, NorESM1-M	HadREM3-GA7-05	time-evolving
SMHI	NorESM1-M	RCA4	constant

The aerosol forcing according to ref. 24. is also indicated.

Data availability

ERA5 data is publicly available from <https://doi.org/10.24381/cds.143582cf>, E-OBS from <https://www.ecad.eu/download/ensembles/download.php>, GEBA data is freely available upon registration from <https://geba.ethz.ch/data-retrieval.html>, CMIP6 data is accessible through <https://wcrp-cmip.org/cmip-data-access/>, and CORDEX simulations through <https://cordex.org/data-access/esgf/>.

Code availability

The code used to perform the dynamical adjustment can be obtained from <https://zenodo.org/records/10040950>. Additional code for remaining analyses is available from the corresponding author upon request.

Received: 31 August 2023; Accepted: 19 March 2024;

Published online: 06 April 2024

References

- van den Hurk, B. et al. The match between climate services demands and Earth System Models supplies. *Clim. Serv.* **12**, 59–63 (2018).
- Allis, E. et al. The Future of Climate Services. *WMO Bull.* **68**, 50–58 (2019).
- IPCC, 2021: Climate Change 2021: The Physical Science Basis. Contribution of Working Group I to the Sixth Assessment Report of the Intergovernmental Panel on Climate Change (eds Masson-Delmotte, V., et al.). Cambridge University Press, Cambridge, United Kingdom and New York, NY, USA, 2391 pp. <https://doi.org/10.1017/9781009157896>.
- Seneviratne, S. I. et al. 2021: Weather and Climate Extreme Events in a Changing Climate. In Climate Change 2021: The Physical Science Basis. Contribution of Working Group I to the Sixth Assessment Report of the Intergovernmental Panel on Climate Change (eds Masson-Delmotte, V., P. Zhai, A. Pirani, S. L. Connors, C. Péan, S. Berger, N. Caud, Y. Chen, L. Goldfarb, M. I. Gomis, M. Huang, K. Leitzell, E. Lonnoy, J. B. R. Matthews, T. K. Maycock, T. Waterfield, O. Yelekçi, R. Yu, and B. Zhou). Cambridge University Press, Cambridge, United Kingdom and New York, NY, USA, 1513–1766. <https://doi.org/10.1017/9781009157896.013>.
- Ranasinghe, R. et al. 2021: Climate Change Information for Regional Impact and for Risk Assessment. In Climate Change 2021: The Physical Science Basis. Contribution of Working Group I to the Sixth Assessment Report of the Intergovernmental Panel on Climate Change [Masson-Delmotte, V., P. Zhai, A. Pirani, S. L. Connors, C. Péan, S. Berger, N. Caud, Y. Chen, L. Goldfarb, M. I. Gomis, M. Huang, K. Leitzell, E. Lonnoy, J. B. R. Matthews, T. K. Maycock, T. Waterfield, O. Yelekçi, R. Yu, and B. Zhou (eds)]. Cambridge University Press, Cambridge, United Kingdom and New York, NY, USA, 1767–1926. <https://doi.org/10.1017/9781009157896.014>.
- Gutiérrez, J. M. et al. 2021: Atlas. In Climate Change 2021: The Physical Science Basis. Contribution of Working Group I to the Sixth Assessment Report of the Intergovernmental Panel on Climate Change (eds Masson-Delmotte, V., P. Zhai, A. Pirani, S. L. Connors, C. Péan, S. Berger, N. Caud, Y. Chen, L. Goldfarb, M. I. Gomis, M. Huang, K. Leitzell, E. Lonnoy, J. B. R. Matthews, T. K. Maycock, T. Waterfield, O. Yelekçi, R. Yu, and B. Zhou). Cambridge University Press, Cambridge, United Kingdom and New York, NY, USA, 1927–2058 <https://doi.org/10.1017/9781009157896.021>.
- Balaji, V., Couvreur, F. & Deshayes, J. Are general circulation models obsolete? *Proc. Natl. Acad. Sci. USA* **119**, e2202075119 (2022).
- Sørland, S. L., Schär, C., Lüthi, D. & Kjellström, E. Bias patterns and climate change signals in GCM-RCM model chains. *Environ. Res. Lett.* **13**, 074017 (2018).
- Iles, C. E. et al. The benefits of increasing resolution in global and regional climate simulations for European climate extremes. *Geosci. Model Dev.* **13**, 5583–5607 (2020).
- Ban, N. et al. The first multi-model ensemble of regional climate simulations at kilometer-scale resolution, part I: evaluation of precipitation. *Clim. Dyn.* **57**, 275–302 (2021).
- Soares, P. M. M. et al. The added value of km-scale simulations to describe temperature over complex orography: the CORDEX FPS-Convection multi-model ensemble runs over the Alps. *Clim. Dyn.* 1–24 (2022).
- Sangelantoni, L. et al. Investigating the representation of heatwaves from an ensemble of km-scale regional climate simulations within CORDEX-FPS convection. *Clim. Dyn.* 1–37 (2023).
- Termonia, P. et al. The CORDEX.be initiative as a foundation for climate services in Belgium. *Clim. Serv.* **11**, 49–61 (2018).
- Lowe, J. A. et al. UKCP18 Science Overview Report, November 2018 (updated March 2019). MetOffice, 1–73 (2018).
- Fischer, A. et al. Climate Scenarios for Switzerland CH2018 – Approach and Implications. *Clim. Serv.* **26**, 100288 (2022).
- Hübener, H. et al. ReKliEs-De (Regionale Klimaprojektionen Ensemble für Deutschland) Ergebnisbericht. World Data Center for Climate (WDCC) at DKRZ, 1–76 (2017).
- Flato, G. et al. Evaluation of Climate Models. in *Climate Change 2013: The Physical Science Basis. Contribution of Working Group I to the Fifth Assessment Report of the Intergovernmental Panel on Climate Change*. Cambridge University Press, Cambridge, United Kingdom and New York, NY, USA (2013).
- Giorgi, F., Jones, C. & Asrar, G. R. Addressing climate information needs at the regional level: the CORDEX Framework. *WMO Bull.* **58**, 175–183 (2009).
- Jacob, D. et al. EURO-CORDEX: new high-resolution climate change projections for European impact research. *Reg. Environ. Change* **14**, 563–578 (2014).
- Jacob, D. et al. Regional climate downscaling over Europe: perspectives from the EURO-CORDEX community. *Reg. Environ. Change* **20**, 51 (2020).
- World Meteorological Organization (WMO). State of the Climate in Europe 2022. WMO-No. 1320, 1–40 (2023).
- Lorenz, R., Stalhandske, Z. & Fischer, E. M. Detection of a climate change signal in extreme heat, heat stress, and cold in Europe from observations. *Geophys. Res. Lett.* **46**, 8363–8374 (2019).
- Vautard, R. et al. Human contribution to the record-breaking June and July 2019 heatwaves in Western Europe. *Env. Res. Lett.* **15**, 094077 (2020).
- Lorenz, P. & Jacob, D. Validation of temperature trends in the ENSEMBLES regional climate model runs driven by ERA40. *Clim. Res.* **44**, 167–177 (2010).
- Ribes, A. et al. An updated assessment of past and future warming over France based on a regional observational constraint. *Earth Syst. Dynam.* **13**, 1397–1415 (2022).
- Brogli, R., Lund Sørland, S., Kröner, N. & Schär, C. Future summer warming pattern under climate change is affected by lapse-rate changes. *Weather Clim. Dynam.* **2**, 1093–1110 (2021).
- Philipona, R., Behrens, K. & Ruckstuhl, C. How declining aerosols and rising greenhouse gases forced rapid warming in Europe since the 1980s. *Geophys. Res. Lett.* **36**, L02806 (2009).
- Wild, M., Wacker, S., Yang, S. & Sanchez-Lorenzo, A. Evidence for clear-sky dimming and brightening in central Europe. *Geophys. Res. Lett.* **48**, e2020GL092216 (2021).
- Freychet, N., Tett, S. F. B., Bolasina, M., Wang, K. C. & Hegerl, G. The local aerosol emission effect on surface shortwave radiation and temperatures. *J. Adv. Model. Earth Syst.* **11**, 806–817 (2019).
- Tang, Q., Leng, G. & Groisman, P. Y. European hot summers associated with a reduction of cloudiness. *J. Clim.* **25**, 3637–3644 (2012).
- Bartók, B. et al. Projected changes in surface solar radiation in CMIP5 global climate models and in EURO-CORDEX regional climate models for Europe. *Clim. Dyn.* **49**, 2665–2683 (2017).
- Gutiérrez, C. et al. Future evolution of surface solar radiation and photovoltaic potential in Europe: investigating the role of aerosols. *Env. Res. Lett.* **15**, 034035 (2020).

33. Boé, J., Somot, S., Corre, L. & Nabat, P. Large discrepancies in summer climate change over Europe as projected by global and regional climate models: causes and consequences. *Clim. Dyn.* **54**, 2981–3002 (2020).
34. Nabat, P., Somot, S., Mallet, A., Sanchez-Lorenzo, A. & Wild, M. Contribution of anthropogenic sulfate aerosols to the changing Euro-Mediterranean climate since 1980. *Geophys. Res. Lett.* **41**, 5605–5611 (2014).
35. Sutton, R. T. & Hodson, D. L. R. Atlantic ocean forcing of North American and European summer climate. *Science* **309**, 115–118 (2005).
36. O'Reilly, C. H., Woollings, T. & Zanna, L. The dynamical influence of the atlantic multidecadal oscillation on continental climate. *J. Clim.* **30**, 7213–7230 (2017).
37. Iles, C. & Hegerl, G. Role of the North Atlantic oscillation in decadal temperature trends. *Environ. Res. Lett.* **12**, 114010 (2017).
38. Delworth, T. et al. The North Atlantic oscillation as a driver of rapid climate change in the Northern Hemisphere. *Nat. Geosci.* **9**, 509–512 (2016).
39. Rousi, E., Kornhuber, K., Beobide-Arsuaga, G., Luo, F. & Coumou, D. Accelerated western European heatwave trends linked to more-persistent double jets over Eurasia. *Nat. Comm.* **13**, 3851 (2022).
40. Trenberth, K. E., Fasullo, J. T. & Shepherd, T. G. Attribution of climate extreme events. *Nat. Clim. Change* **5**, 725–730 (2015).
41. Eyring, V. et al. Human Influence on the Climate System. in *Climate Change 2021: The Physical Science Basis. Contribution of Working Group I to the Sixth Assessment Report of the Intergovernmental Panel on Climate Change*. Cambridge University Press, Cambridge, United Kingdom and New York, NY, USA, 423–552 (2021).
42. Deser, C., Terray, L. & Phillips, A. S. Forced and internal components of winter air temperature trends over North America during the past 50 Years: mechanisms and Implications. *J. Clim.* **29**, 2237–2258 (2016).
43. Lehner, F. & Deser, C. Origin, importance, and predictive limits of internal climate variability. *Environ. Res.: Climate* **2**, 023001 (2023).
44. Vautard, R. et al. Heat extremes in Western Europe increasing faster than simulated due to atmospheric circulation trends. *Nat. Commun.* **14**, 6803 (2023).
45. Vicedo-Cabrera, A. M. et al. The burden of heat-related mortality attributable to recent human-induced climate change. *Nat. Clim. Change* **11**, 492–500 (2021).
46. Coppola, E. et al. Assessment of the European climate projections as simulated by the large EURO-CORDEX regional and global climate model ensemble. *J. Geophys. Res. Atmos.* **126**, e2019JD032356 (2021).
47. Lenderink, G. et al. Summertime inter-annual temperature variability in an ensemble of regional model simulations: analysis of the surface energy budget. *Climatic Change* **81**, 233–247 (2007).
48. Yang, Y., Lou, S., Wang, H., Wang, P. & Liao, H. Trends and source apportionment of aerosols in Europe during 1980–2018. *Atmos. Chem. Phys.* **20**, 2579–2590 (2020).
49. Persad, G. et al. Rapidly evolving aerosol emissions are a dangerous omission from near-term climate risk assessments. *Env. Res. Lett. Clim.* **2**, 032001 (2023).
50. Taranu, I. S. et al. Mechanisms behind large-scale inconsistencies between regional and global climate model-based projections over Europe. *Clim. Dyn.* **60**, 3813–3838 (2023).
51. Schwingshackl, C., Hirschi, M. & Seneviratne, S. I. Global contributions of incoming radiation and land surface conditions to maximum near-surface air temperature variability and trend. *Geophys. Res. Lett.* **45**, 5034–5044 (2018).
52. Sousa, P. M., Trigo, R. M., Barriopedro, D., Soares, P. M. M. & Santos, J. A. European temperature responses to blocking and ridge regional patterns. *Clim. Dyn.* **50**, 457–477 (2018).
53. Nabat, P. et al. Modulation of radiative aerosols effects by atmospheric circulation over the Euro-Mediterranean region. *Atmos. Chem. Phys.* **20**, 8315–8349 (2020).
54. Doblas-Reyes, F. J. et al. Linking global to regional climate change. in *Climate Change 2021: The Physical Science Basis. Contribution of Working Group I to the Sixth Assessment Report of the Intergovernmental Panel on Climate Change*. Cambridge University Press, Cambridge, United Kingdom and New York, NY, USA, pp. 1363–1512 (2021).
55. Thompson, V. et al. The most at-risk regions in the world for high-impact heatwaves. *Nat. Comm.* **14**, 2152 (2023).
56. di Virgilio, G. et al. Selecting CMIP6 GCMs for CORDEX dynamical downscaling: model performance, independence, and climate change signals. *Earth's Future* **10**, e2021EF002625 (2022).
57. Iturbide, M. et al. An update of IPCC climate reference regions for subcontinental analysis of climate model data: definition and aggregated datasets. *Earth Sys. Sci. Data* **12**, 2959–2970 (2020).
58. Hersbach, H. et al. The ERA5 global reanalysis. *Q. J. R. Meteorol. Soc.* **146**, 1999–2049 (2020).
59. Bell, B. et al. The ERA5 global reanalysis: preliminary extension to 1950. *Q. J. R. Meteorol. Soc.* **146**, 4186–4227 (2021).
60. Lamarque, J.-F. et al. Historical (1850–2000) gridded anthropogenic and biomass burning emissions of reactive gases and aerosols: methodology and application. *Atmos. Chem. Phys.* **10**, 7017–7039 (2010).
61. Hersbach, H. et al. ERA-20CM: a twentieth-century atmospheric model ensemble. *Q. J. R. Meteorol. Soc.* **141**, 2350–2375 (2015).
62. Cornes, R. C., van der Schrier, G., van den Besselaar, E. J. M. & Jones, P. D. An ensemble version of the E-OBS temperature and precipitation data sets. *J. Geophys. Res. Atmos.* **123**, 9391–9409 (2018).
63. Wild, M. et al. The Global Energy Balance Archive (GEBA) version 2017: a database for worldwide measured surface energy fluxes. *Earth Syst. Sci. Data* **9**, 601–613 (2017).
64. Eyring, V. et al. Overview of the Coupled Model Intercomparison Project Phase 6 (CMIP6) experimental design and organization. *Geosci. Model Dev.* **9**, 1937–1958 (2016).
65. Taylor, K. E., Stouffer, R. J. & Meehl, G. A. An Overview of CMIP5 and the experiment design. *Bull. Am. Meteorol. Soc.* **93**, 485–498 (2012).
66. Dee, D. P. et al. The ERA-Interim reanalysis: configuration and performance of the data assimilation system. *Q. J. R. Meteor. Soc.* **137**, 553–597 (2011).
67. Sippel, S. et al. Uncovering the forced climate response from a single ensemble member using statistical learning. *J. Clim.* **32**, 5677–5699 (2019).
68. Singh, J., Sippel, S. & Fischer, E. M. Circulation dampened heat extremes intensification over the Midwest USA and amplified over Western Europe. *Commun Earth Environ* **4**, 432 (2023).
69. Zhuang, Y., Fu, R., Santer, B. D., Dickinson, R. E. & Hall, A. Quantifying contributions of natural variability and anthropogenic forcings on increased fire weather risk over the western United States. *Proc. Natl. Acad. Sci. USA* **118**, e2111875118 (2021).
70. Rodgers, K. B. et al. Ubiquity of human-induced changes in climate variability. *Earth Syst. Dyn.* **12**, 1393–1411 (2021).

Acknowledgements

This study was partly supported by the European Union's Horizon 2020 research and 457 innovation programme under grant agreement No. 101003469 (XAIDA project). We acknowledge the E-OBS dataset from the EU-FP6 project UERRA and the Copernicus Climate Change Service, and the data providers in the ECA&D project. GEBA is co-funded by the Federal Office of Meteorology and Climatology MeteoSwiss within the framework of GCOS Switzerland. We also acknowledge the CESM2 Large Ensemble Community Project and supercomputing resources provided by the IBS Center for Climate Physics in South Korea. We acknowledge the World Climate Research Programme, which, through its Working Group on Coupled Modeling, coordinated and promoted CMIP6. We thank the climate modeling groups for producing and making available their model output, the Earth System Grid Federation (ESGF) for archiving the data and providing access, and the multiple funding

agencies who support CMIP6 and ESGF. We thank Urs Beyerle for downloading and curating the CMIP6 data at ETH Zurich, and also thank Martin Hirschi and Michael Sprenger for providing ERA5 data. Furthermore, we acknowledge the World Climate Research Programme's Working Group on Regional Climate, and the Working Group on Coupled Modeling, former coordinating body of CORDEX and responsible panel for CMIP5. We also thank the climate modeling groups for producing and making available their model output, and the ESGF for storing and providing the data.

Author contributions

D.L.S. and J.S. processed the data, and M.H. provided the tools to post-process CMIP6 output. D.L.S. and J.S. conducted the main analysis, J.S. performed the dynamical adjustment, and D.L.S. created the figures. M.W. and D.L.S. performed and interpreted the GEBA analysis together. D.L.S., J.S., M.H., E.M.F. and S.I.S. designed the study. All authors wrote the manuscript. S.I.S. and E.M.F. conceived the study.

Funding

Open access funding provided by Swiss Federal Institute of Technology Zurich.

Competing interests

The authors declare no competing interests.

Additional information

Supplementary information The online version contains supplementary material available at <https://doi.org/10.1038/s43247-024-01332-8>.

Correspondence and requests for materials should be addressed to Dominik L. Schumacher.

Peer review information *Communications Earth & Environment* thanks Mika Rantanen and the other, anonymous, reviewer(s) for their contribution to the peer review of this work. Primary Handling Editors: Mengze Li, Heike Langenberg. A peer review file is available.

Reprints and permissions information is available at <http://www.nature.com/reprints>

Publisher's note Springer Nature remains neutral with regard to jurisdictional claims in published maps and institutional affiliations.

Open Access This article is licensed under a Creative Commons Attribution 4.0 International License, which permits use, sharing, adaptation, distribution and reproduction in any medium or format, as long as you give appropriate credit to the original author(s) and the source, provide a link to the Creative Commons licence, and indicate if changes were made. The images or other third party material in this article are included in the article's Creative Commons licence, unless indicated otherwise in a credit line to the material. If material is not included in the article's Creative Commons licence and your intended use is not permitted by statutory regulation or exceeds the permitted use, you will need to obtain permission directly from the copyright holder. To view a copy of this licence, visit <http://creativecommons.org/licenses/by/4.0/>.

© The Author(s) 2024